Micro/Nanoscale Spatial Resolution Temperature Probing for the Interfacial Thermal Characterization of Epitaxial Graphene on 4H-SiC

*Yanan Yue, Jingchao Zhang, and Xinwei Wang**

Limited internal phonon coupling and transfer within graphene in the out-of-plane direction significantly affects graphene–substrate interfacial phonon coupling and scattering, and leads to unique interfacial thermal transport phenomena. Through the simultaneous characterization of graphene and SiC Raman peaks, it is possible, for the first time, to distinguish the temperature of a graphene layer and its adjacent 4H-SiC substrate. The thermal probing resolution reaches the nanometer scale with the graphene (≈1.12 nm) and is on the micrometer scale (≈12 μm) within SiC next to the interface. A very high thermal resistance at the interface of $5.30^{+0.46}_{-0.46} \times 10^{-5}$ K m^2 W^{-1} is observed by using a Raman frequency method under surface Joule heating. This value is much higher than those from molecular dynamics predictions of $7.01^{+1.05}_{-1.05} \times 10^{-1}$ and $8.47^{+0.75}_{-0.75} \times 10^{-10}$ K m^2 W^{-1} for surface heat fluxes of 3×10^9 and 1×10^{10} W m^{-2}, respectively. This analysis shows that the measured anomalous thermal contact resistance stems from the thermal expansion mismatch between graphene and SiC under Joule heating. This mismatch leads to interface delamination/separation and significantly enhances local phonon scattering. An independent laser-heating experiment conducted under the same conditions yielded a higher interfacial thermal resistance of $1.01^{+1.23}_{-0.59} \times 10^{-4}$ K m^2 W^{-1}. Furthermore, the peak width method of Raman thermometry is also employed to evaluate the interfacial thermal resistance. The results are 3.52×10^{-5} and 8.57×10^{-5} K m^2 W^{-1} for Joule-heating and laser-heating experiments, respectively, confirming the anomalous thermal resistance between graphene and SiC. The difference in the results from the frequency and peak-width methods is caused by the thermal stress generated in the heating processes.

1. Introduction

Graphene has attracted significant attention due to its unique characteristics, which include electric-field effects, the quantum Hall effect, and a high charge-carrier mobility.[1] Its excellent thermophysical properties prompt potential applications in semiconductor devices such as field-effect transistors (FETs) and sensors.[2] The high thermal conductivity of graphene has been measured to be between 630 and 5300 W m^{-1} K^{-1}. This wide range comes from both the difference in experimental conditions and graphene samples, including the temperature rise in the measurement, the difference in suspended and supported graphene, and graphene with different layer numbers and inner structures.[2d,3] Theoretical analyses and molecular dynamics simulations have been conducted to verify these high values.[4] Heat dissipation in the in-plane direction would be greatly impeded by the high thermal resistance due to the low thickness of graphene (0.335 nm for a single layer).[2d,3a] In its

Dr. Y. Yue, J. Zhang, Prof. X. Wang
Department of Mechanical Engineering
2025 Black Engineering Building
Iowa State University
Ames, IA, 50011-2161, USA
E-mail: xwang3@iastate.edu

DOI: 10.1002/smll.201101598

© 2011 Wiley-VCH Verlag GmbH & Co. KGaA, Weinheim

applications, a graphene sheet is often attached to a substrate, in which case thermal transport through the graphene–substrate interface provides an alternative pathway for heat dissipation. Therefore, knowledge of the thermal resistance at the interface between graphene and an adjacent material is important to evaluate out-of-plane heat dissipation.

In graphene fabrication, two approaches are frequently used: mechanical cleavage and epitaxial growth on SiC.[1a,1b,5] The mechanical cleavage method is an easy and effective way to make samples by tape tearing, while the bonding between graphene and substrate is through van der Waals forces and as such only small-sized samples can be made.[5a] Growing epitaxial graphene on SiC requires annealing temperatures higher than 1200 °C, but permits bigger samples to be fabricated as well as covalent bonding between graphene and SiC.[6] This kind of bonding exhibits metallic or semiconductive characteristics, which is very effective for phonon transport.[6b] In this work, epitaxial graphene grown on a 4H-SiC substrate is used to explore phonon transport across the interface and measure the local thermal contact resistance.

For the heat dissipation from graphene-based field-effect transistors to the substrate, Freitag et al. conducted early experimental work on probing the temperature of graphene using Raman thermometry with different Joule heating applied to the graphene. This work pioneered the study of heat dissipation from graphene to substrate, however no graphene–substrate interfacial thermal resistance was explored.[7] Work by Panzer et al. investigated the thermal resistance between low-dimensional nanostructures and semi-infinite media.[8] Their work focused only on the interface between ideal and artificial harmonic 1D and 3D fcc lattices. Most recently, Chen et al. performed experiments to characterize the thermal contact resistance between graphene and SiO_2.[9] They made a graphene sample sandwiched between two SiO_2 layers with one side patterned with an electrical circuit (Au) and used the 3ω technique to characterize the thermal contact resistance. The excellence of this design avoided the effect of the nonlinear I–V characteristic of graphene-based circuits.[9] The work by Schmidt et al. investigated the thermal interfacial conductance of metal-coated HOPG (highly oriented pyrolytic graphite) by using the time-domain thermoreflectance method. Due to the different adhesion effects, measured values vary from 20 to 120 MW m^{-2} K^{-1} in the temperature range 100–300 K for different coated metal materials.[10] In this work a novel method that combines simultaneous Raman spectroscopy and Joule heating for temperature mapping is established to characterize the thermal contact resistance between graphene and SiC. Here the temperature of graphene can be distinguished from that of the SiC substrate and phonon transport can be evaluated across the interfacial region.

2. Results

2.1. The Joule-heating experiment

Raman thermometry has been broadly applied to the temperature and thermophysical property measurements of different materials, such as silicon and carbon nanotubes (CNTs).[11] In 2008, for the first time Balandin et al. used this method, combined with laser heating, to successfully measure the thermal conductivity of a suspended single layer of graphene.[2d] Raman thermometry is based on the physics that phonon frequencies and lifetimes induced from the anharmonicity in interatomic potentials are temperature-dependent. The intensity, frequency (Raman shift), and width of the Raman peak will change with temperature.[12] In Raman thermometry, the frequency method features high sensitivity and is often employed in temperature measurements. The peak intensity-based method has a high sensitivity as well but is significantly affected by the focusing level shift due to thermal expansion effects. In this experiment, because the focal spot of laser probe is quite small, small changes to the focal level would greatly affect the Raman intensity. Therefore, the frequency method is primarily employed for temperature measurements and thermal transport characterization.

Graphene is easily penetrated by the probing laser because of its optical transparency at the probe wavelength of 532 nm, wherein the spontaneous Raman mapping consists of the signal of both graphene and substrate. In a Raman spectrum, there are three peaks to identify graphene in the range from 0 to 3000 cm^{-1}: D-band ≈1330 cm^{-1}, G-band ≈1580 cm^{-1}, and 2D-band (G' band in some literatures) ≈2700 cm^{-1}, and two peaks for SiC: the E_2 (transverse optical, TO) mode ≈780 cm^{-1} and its second-order peak at ≈1530 cm^{-1}.[13] The D-band of graphene reflects the structural quality of the sample, while the G-band is caused by the Raman active E_{2g} phonon, and the 2D-band contains the information about the absence of the D-band.[14] The temperature-dependence of the Raman signal is an intrinsic characteristic of these materials, and the selection of peaks for temperature sensing depends on the significance of peak intensity and the distinguishable Raman shift.

To characterize the thermal contact resistance between graphene and SiC, their temperature difference should be primarily determined. As shown in **Figure 1**, for the experimental principle, an epitaxial graphene sheet grown on a SiC substrate is connected with two electrodes. An electrical current is passed through the graphene to induce steady-state Joule heating. At the same time, a confocal micro-Raman experiment is conducted by irradiating the central area of the graphene layer with an excitation laser. Based on the measured Raman signal, the temperature of the graphene sheet and the SiC substrate can be distinguished simultaneously with subnanometer spatial resolution in the vertical direction. The interfacial thermal resistance can be readily determined from $R_{tc} = (T_{graphene} - T_{SiC})\,(I^2 R)$, where A is the graphene area, R is its electrical resistance, and I is the applied current. The heat generated from Joule heating is dissipated in two directions: one part crosses the plane to the interface and the other part dissipates along the graphene layer. In the Joule-heating experiment, the second part is negligible because the heating is uniform and almost no temperature gradient exists in the in-plane direction.

The layer number of graphene needs to be identified since the temperature coefficient would be different for samples with different layers.[15] Raman spectroscopy is demonstrated as an effective tool to determine layer numbers

© 2011 Wiley-VCH Verlag GmbH & Co. KGaA, Weinheim

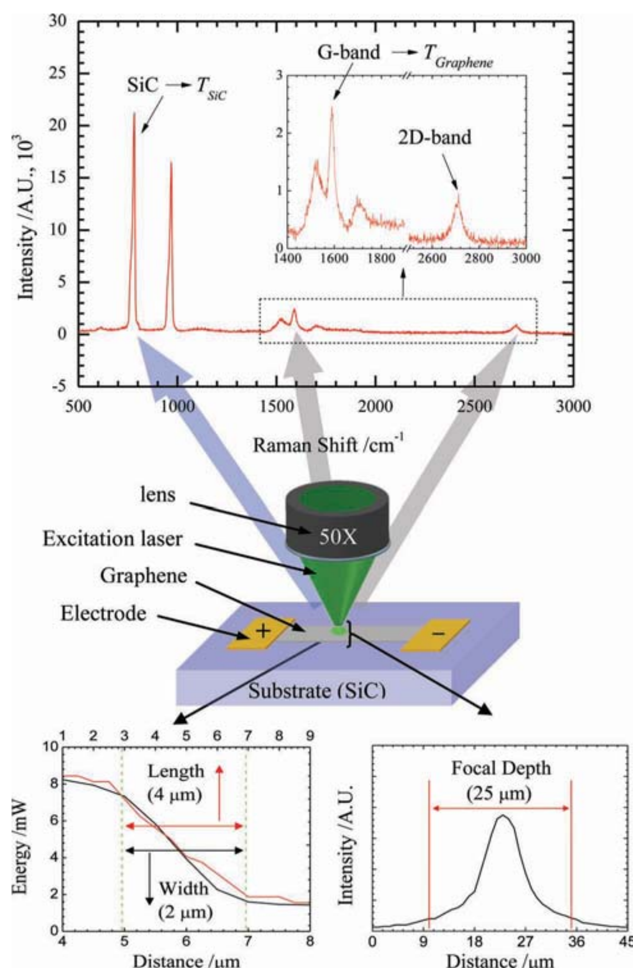

Figure 1. Principle of the Joule-heating experiment used for the thermal-contact-resistance measurements. The spot size of the laser is measured by using a blade on a microstage of 4 μm × 2 μm, as shown in the bottom left panel. The bottom right panel shows that the focal depth of lens is determined as 25 μm from the evolution of Raman intensity when the lens approaches the sample. The top figure depicts the Raman spectrum of epitaxial graphene on 4H-SiC (000$\bar{1}$). The graphene is determined to have three layers from the intensity ratio between the G-band and the 2D-band.

using the intensity of the G-band and the 2D-band.[14,16] The 2D-band is very sensitive to the layer number because the change of the electronic structure of graphene affects the double resonance effect, with the peak of the 2D-band broadening and becoming less symmetric as the layer number increases.[13a,14,16,17] Meanwhile, the intensity of the G-band linearly increases with layer number over a small range of layers.[14] The Raman spectrum of our sample, shown in Figure 1, shows that the 2D-band exhibits a symmetric shape with a sharp peak while the G-band is less than twice height of the 2D-band. The graphene is identified to have tri-layers, using the 532 nm laser. Moreover, the D-band does not appear in the spectrum, confirming the high structural quality of the sample.

The temperature coefficients of graphene and 4H-SiC are calibrated individually from room temperature to 250 °C. Among the Raman peaks of graphene, the G-band is preferred for temperature determination due to the high intensity and distinguishable peak position. The E_2 peak of SiC has a high intensity induced by its crystalline structure. Due to the resolution limit of the spectrometer, the precise peak location is determined by fitting the Raman peak with a Gaussian function. The second order E_2 mode Raman of SiC at 1530 cm^{-1} is very weak and partly overlaps with the G-band of graphene. They are resolved by using double-peak fitting, shown in **Figure 2**. Although the dependence of the Raman shift on temperature is nonlinear due to the different phonon interactions arising from the complicated interatomic potentials, this relationship can be approximately considered as linear over the small temperature range investigated here with little uncertainty.[15] The relationship between peak frequency and temperature are shown in Figure 2. The slopes of the linear fits are -0.016 and -0.025 cm^{-1} °C^{-1} for the E_2 mode of SiC and the G-band of graphene, respectively. The Raman shift is also affected by the number of graphene layers, presenting itself as a downshift as the layer number increases.[14] In our experiment, the sample was firmly placed on a microstage, and the same point was measured as guaranteed from the temperature calibrations for the Joule heating and laser-heating experiments. In addition, the sample has three layers at the measurement point, and uniformity over the surrounding region was confirmed. In the measurement, the shift of measured point during the experiment is carefully controlled such that it does not exceed the region of three layers.

Harima et al. measured the temperature coefficient of 6H-SiC and obtained a slope of around –0.023 cm^{-1} °C^{-1} in the temperature range 0–1000 °C.[18] The work by Calizo et al. obtained the temperature coefficient of G-band of graphene as –0.016 cm^{-1} °C^{-1} for a single layer and –0.015 cm^{-1} °C^{-1} for bilayer using a 488 nm laser.[15] It has been proved that the temperature coefficient varies with the number of graphene layers. Other work by Zhang et al. and Allen et al. got slopes

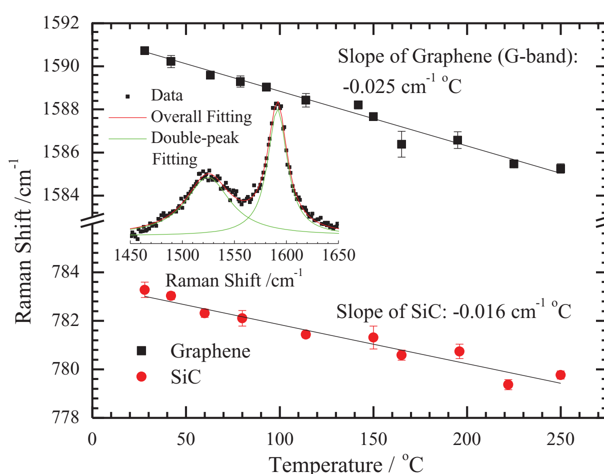

Figure 2. The temperature dependence of the Raman shift for silicon carbide and the G-band of graphene. The Raman shift position is determined from the double-peak fitting using a Gaussian function. This fitting takes into account the overlap effect of the SiC peak centered at 1530 cm^{-1}. The slopes of linear fitting are -0.016 and –0.025 cm^{-1} °C^{-1} for SiC and graphene, respectively.

© 2011 Wiley-VCH Verlag GmbH & Co. KGaA, Weinheim

ranging from –0.0186 to –0.038 cm^{-1} °C^{-1} for the G-band using different lasers.[19] Since the temperature dependence of the frequency shift is determined by the inharmonic interaction of the phonons, the coefficients are different for materials with different structures or if different probing lasers are used.[15,18,20] Over a small temperature range, the relationship between temperature and Raman frequency can be regarded as linear.[15] The variation in the temperature coefficients can also be due to the different temperature ranges used in the calibration. For example, the temperature coefficient of silicon is small over a low temperature range but larger as the temperature increases.[21] The temperature coefficient of the G-band of graphene measured in Calizo et al.'s work over a low temperature range is smaller than our value,[15] and it is reasonable for our measurement to obtain a larger slope, since the measurement is conducted over a higher temperature range. Therefore, our calibration result is in good agreement with others, considering the variance of the experimental conditions employed here.

As mentioned above, the thermal resistance at the graphene–SiC interface is expressed as $R_{tc} = (T_{graphene} - T_{SiC})/(I^2 R)$. To obtain a sensible temperature difference between the graphene and the SiC a controllable heating energy is applied on the 13.89 mm^2 effective area of the graphene. The results for the relationship between temperature and input power are illustrated in **Figure 3**. Since determination from a single point involves a high degree of uncertainty, several heating densities were applied to the graphene to obtain a sensible temperature difference. To improve the accuracy of the measurement a linear fit of the relationships between temperature and power may be conducted. The thermal resistance is calculated by combining the slope difference of the fittings and the sample area as $R_{tc} = (T'_{graphene} - T'_{SiC}) \cdot A$, where $T'_{graphene}$ and T'_{SiC} are the temperature against heating power slopes shown in Figure 3.

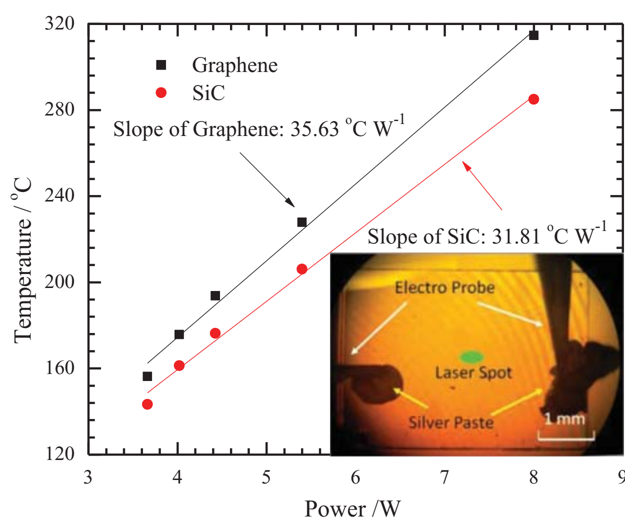

Figure 3. The result of Joule heating for the relationship between temperature and heating power. The interfacial thermal resistance is determined from the slope difference to be $5.30^{+0.46}_{-0.46} \times 10^{-5}$ Km ^{2} W $^{-1}$. The heat conduction resistance of the SiC layer is found to have a negligible effect on the measurement.

R_{tc} is calculated as $5.30^{+0.46}_{-0.46} \times 10^{-5}$ Km^2 W^{-1}, where the uncertainty comes from the linear fit of the temperature difference. This value also includes the heat-conduction resistance in the SiC substrate, since the measured temperature of SiC is not exactly from the surface of substrate but rather integrated over the whole focal depth. As shown in Figure 1, the focal depth of the lens is 25 μm. The thermal conductivity of 4H-SiC is 390 W K^{-1} m^{-1} as provided by the supplier. Assuming the temperature of SiC is obtained from the middle point of the focal depth, the heat conduction resistance in 4H-SiC is calculated to be 3.21×10^{-8} K m^2 W^{-1}. This heat-conduction resistance is very small compared with the measured total resistance of $5.30^{+0.46}_{-0.46} \times 10^{-5}$ Km^2 W^{-1}, and can be neglected. Our measured interfacial thermal resistance is much higher than the values other people measured for graphene on other substrate materials. In Chen et al.'s work, the contact resistance between graphene and silicon dioxide, measured using the 3ω method, ranges from 5.6×10^{-9} to 1.2×10^{-8} K m^2 W^{-1}.[9] Lyeo et al. measured the thermal-contact resistance of the interfaces between highly dissimilar materials to be around 3×10^{-8} K m^2 W^{-1}.[22] Normally, the covalent bonding between epitaxial graphene and SiC is expected to greatly reduce the thermal resistance. It is therefore suspected that there is an anomalous phenomenon involved at the interface during our measurements.

2.2. Molecular Dynamics Simulations

To help interpret the experimental results, Molecular Dynamics (MD) simulations were conducted to check the graphene–SiC interfacial thermal resistance. The MD simulation uses the Tersoff potential to describe C–C, C–Si, and Si–Si interactions. Periodic boundary conditions are applied on four sides of the sample. Initially, a single square layer of graphene with side lengths of 2 nm is placed on the top of a bulk 4H-SiC, which is set to be $25.8 \times 23.1 \times 30.1$ Å in the x, y, and z directions, respectively. A total of 2170 atoms, including 170 atoms in the graphene layer and 2000 atoms of bulk SiC, are involved in the system. The clearance between the graphene and the SiC surface is initially set at 0.21 nm. During the initial 1.5 ns simulation, NVT (canonical ensemble) control is used for all atoms to make the system reach its equilibrium state at 300 K. NVE (microcanonical ensemble) control is then used for the following 300 ps before applying heating. A time step of 0.5 fs is used in this simulation. In order to construct a temperature difference (denoted as ΔT) between the graphene layer and the bulk SiC, a heat flux q is added on the graphene layer while subtracting the same heat flux from the two bottom layers of bulk SiC, as delineated in **Figure 4**. Heat addition and subtraction are performed every second time step by changing the nontranslational kinetic energy of groups of atoms whose aggregate momentums are conserved. The thermal energy added to and subtracted from the system is equal. Therefore, the total energy of the system is conserved without any artificial forces. The temperatures of the graphene (T_G) and the top two layers of bulk SiC (T_{SiC}) are then used to determine the interfacial thermal resistance between graphene and SiC. This thermal resistance is calculated

© 2011 Wiley-VCH Verlag GmbH & Co. KGaA, Weinheim

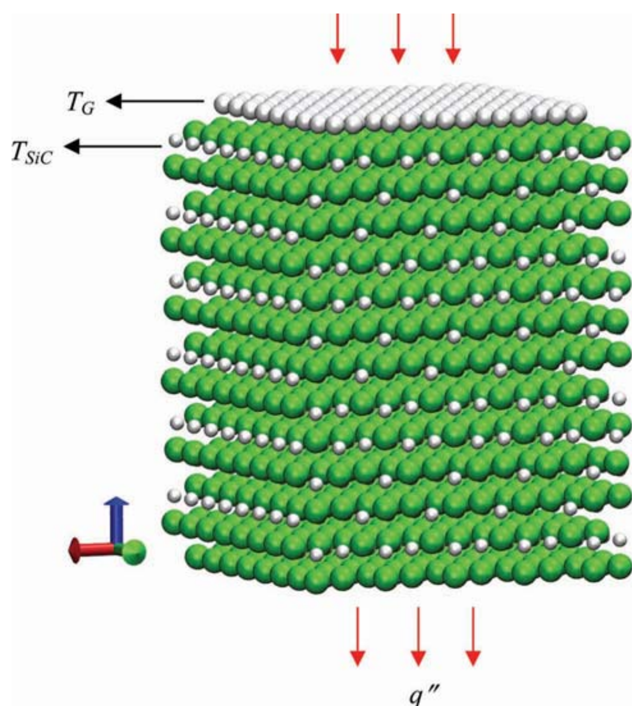

Figure 4. Schematic of the MD simulations of a single layer of graphene on 4H-SiC.

as $\Delta T/q$. A considerable temperature jump over the interface between graphene and bulk SiC is observed in our simulation.

The heat fluxes $q = 3 \times 10^9$ Wm^{-2} and 1×10^{10} W m^{-2} are applied in two different cases, which are heated for 14 ns and 900 ps, respectively. In the first case, the steady-state temperature difference is 2.10 K, and the thermal resistance is calculated to be $7.01^{+1.05}_{-1.05} \times 10^{-10}$ Km^2 W^{-1}. In the second case, the steady-state temperature difference is 8.47 K, and the thermal resistance is $8.47^{+0.75}_{-0.75} \times 10^{-10}$Km^2 W^{-1}. Clearly the result from the simulation is much lower than the experimental value. A detailed discussion of this difference is provided in the following section.

3. Discussion: Experiment Versus Simulation

The mechanically weak interface arising from the manufacturing process is a possible reason for the high the thermal resistance reported in this work. However, it has been demonstrated that the thermal expansion effect of graphene and SiC should be considered when electric heating is applied. Jiang et al. conducted a numerical study using a nonequilibrium Green's function to investigate the expansion coefficient of graphene for different interactions on substrates.[23] The results showed that graphene displayed a high thermal-expansion coefficient in cases where strong interactions with the substrate were present, with the coefficient increasing with temperature.[23] Allen et al. observed and experimentally verified the wrinkling and folding effect of graphene. They attributed the high temperature coefficient of the Raman shift of the G-band in part to the high stress induced by the expansion effect.[19b] A comprehensive analysis of the stress effects of graphene on SiC was conducted by Ni et al. The strong interaction of epitaxial graphene with its substrate due to covalent bonding would result in very high strain stresses, which was verified by the Raman imaging of graphene with different layers.[5a] The epitaxial graphene was expanded rather than compressed due to its smaller lattice constants compared with SiC.[24] The thermal expansion coefficient of 4H-SiC is 4.5×10^{-6} °C^{-1},[25] while that of graphene ranges from negative values to as high as 1×10^{-5} °C^{-1}.[23] It was found that there was a significant difference in the thermal expansion between epitaxial graphene and SiC, which might cause thermal expansion mismatch and separation at the interface.[5a,26] This would add an extra effect on top of the phonon velocity and density mismatch between the two adjacent materials, thereby enhancing the thermal contact resistance.[27]

Figure 5 depicts thermal expansion effect of the sample in the Joule-heating experiment. In this experiment the sample is heated from room temperature to around 300 °C. During this temperature rise, considering the extreme case where the graphene is a whole piece across the SiC substrate, just 1% difference in the thermal expansion coefficients between them will contribute a peeling-off distance at the sample center of around 11.7 μm. This is an extremely high value compared to the thickness of graphene, and one can expect that this effect would greatly enhance the local thermal resistance. For our sample, there is high possibility that the graphene layer consists of several small pieces, but nevertheless the mismatch induced by the different expansion coefficients is still significant.

Since the thermal-expansion coefficient depends on the interactions with adjacent materials the coefficients of each

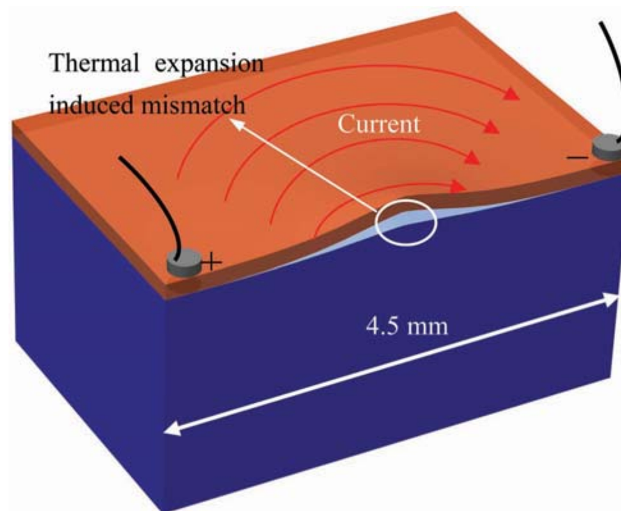

Figure 5. Material thermal response in the Joule-heating experiment. The most severe mismatch happens at the center of the sample (cross-sectional view). Although heating is uniform in graphene, the highest temperature emerges at the center of the sample, inducing the largest thermal expansion, because the edge has more heat transfer to the silicon substrate (across the SiC) and the electrode leads.

© 2011 Wiley-VCH Verlag GmbH & Co. KGaA, Weinheim

of the graphene layers are different due to the nature of their atomic bonding (first layer is covalently bonded while the other two are held by van der Waals forces). This fact was not accounted for in the effect induced by the small temperature gradient in the cross-plane direction of graphene. Taking these effects into consideration, the expansion of different graphene layers would be more or less different. Without considering the thermal-expansion effect, the thermal resistance between different layers is high due to van der Waals forces wherein phonon transport between the layers may be regarded as ballistic.[27] This expansion effect would significantly weaken the phonon interactions between the layers and enhance the originally high thermal resistance. The cross-plane thermal conductivity of HOPG is measured as 6.1 W m^{-1} K^{-1} in Schmidt et al.'s work.[28] In our experiment, the real thermal conductivity between different layers could be much lower than this value due to the thermal-expansion effect.

To verify the measurement discussed above, a laser-heating experiment is conducted to consolidate the Joule-heating result. A probing laser with 8 mW energy can generate local heating as high as 1×10^9 W m^{-2}. For consistency, the same point measured in the Joule-heating experiment is taken for this measurement. The laser focus is precisely adjusted to make the heating energy quantifiable. It is found that the Raman peak shifts significantly to lower wavenumbers as the focal level improves. This is displayed in **Figure 6**, which shows the Raman spectra at different focal levels. Moreover, the Raman signal is strong at lower focal level (less intense heating) and the intensity decreases as the heating effect is enhanced. This is because the high temperature induced by the intensive heating changes the band structure, which restricts the photon interactions necessary to generate the Raman signal.[11,12b]

The absorption of the laser light in the graphene layer can be approximated from Dirac fermions ($\approx \pi e^2/\hbar c$),[29] wherein the absorption is also affected by the temperature. To the best of our knowledge no data on the absorption of graphene over a wide temperature range has been previously reported. Therefore, a value of 2.3% for the absorption by a single layer, which is widely used by many researchers, is used at our wavelength (532 nm).[29,30] The reflectance is less than 0.1%, and can be ignored.[30,31] The heating power also includes the second absorption from the reflection of SiC. At 532 nm, 23% of the laser light irradiated on the 4H-SiC is reflected back into the graphene for further absorption. The light absorption inside the SiC can be ignored.[32] The heating density in the graphene layer is evaluated by assuming all energy is focused in the area of the laser spot. The measured temperature of the graphene is 392 °C, while that of SiC is 197 °C. In the experiment, the relatively high thermal resistance at the interface would cause a large part of the energy to dissipate along the in-plane direction of the graphene layer to other unheated regions. Thermal transport along the graphene layer can be evaluated using the Bessel function.[3b] The physical model for our sample is treated as the case of a fin with a nonuniform cross-sectional area. The heat transfer rate along the in-plane direction of graphene is expressed as[33]

$$q_f = 2\pi k r_1 t \theta_b m \frac{K_1(mr_1) I_1(mr_2) - I_1(mr_1) K_1(mr_2)}{K_0(mr_1) I_1(mr_2) + I_0(mr_1) K_1(mr_2)} \quad (1)$$

where k is thermal conductivity of graphene, r_1 and r_2 are the radius of the heating area of the laser beam and the heat transfer area of the graphene sample, respectively; t is the thickness of graphene, θ_b is the excess temperature of graphene, which can be eliminated in the following thermal resistance calculation: $m = \sqrt{h/kt}$, where h is the effective convection coefficient of the graphene. In this case, it is assumed that all heat dissipates through the interface and no convection from graphene to air is present. Heat dissipation through the interface is equivalently regarded as convective heat loss, thus the value of h is evaluated from the correlation: $1/R_{tc}$, where R_{tc} is thermal-contact resistance measured in the Joule-heating experiment. In the above expression, to calculate heat transfer rate, K_0 and I_0 values are modified zero-order Bessel functions of the first and second kinds while K_1 and I_1 are modified first-order Bessel functions of the first and second kinds, respectively. Assuming the thermal conductivity of graphene is 1000 W m^{-1} K^{-1}, the in-plane thermal resistance is determined as 2.56×10^5 K W^{-1} based on a graphene layer thickness of 1.12 nm (three layers).[34] The overall thermal resistance at the interface within the laser-heating region is evaluated based on the thermal-contact resistance measured in the Joule-heating experiment as 6.62×10^6 K W^{-1}, which is about 26 times higher than the in-plane direction (see **Figure 7**a). Therefore, only 3.7% of the absorbed laser energy would transport directly through to the interface. This explains why the temperature of the graphene measured in the laser-heating experiment is not too much higher than the value in the Joule-heating experiment, despite the fact that a higher heat intensity is applied. The heating power involved to evaluate the thermal contact resistance is 3.13×10^6 W m^{-2} and the thermal resistance is calculated as $6.23^{+1.25}_{-1.25} \times 10^{-5}$ Km^2 W^{-1}. If the thermal conductivity of

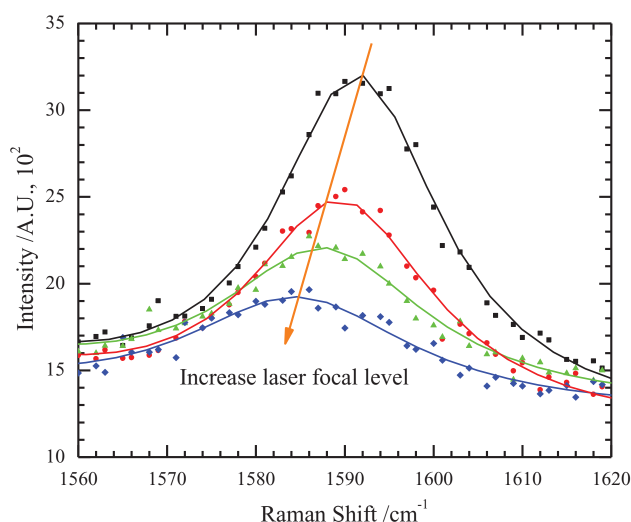

Figure 6. Raman spectra in the laser-heating experiment at different focal levels. The heating intensity from the laser is increased in the direction of the arrow. The Raman peak shifts to lower wavenumbers while its intensity decreases.

© 2011 Wiley-VCH Verlag GmbH & Co. KGaA, Weinheim

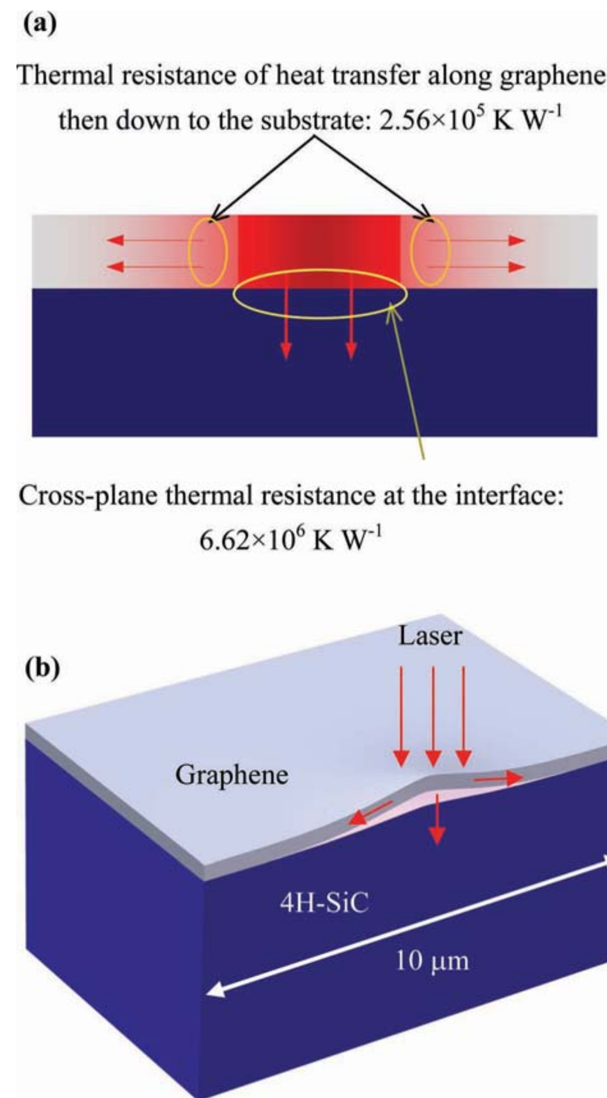

Figure 7. a) Schematic of the thermal resistance calculation of the in-plane and out-of-plane directions: thermal resistance of heat transfer along graphene, then to the substrate, is 2.56×10^5 K W^{-1}, while the cross-plane thermal resistance at the interface is 6.62×10^6 K W^{-1}. These thermal resistances are estimated using the interfacial thermal resistance measured by the Joule-heating experiment, and are intended to demonstrate the heat-transfer analysis conducted in the work. b) Schematic depicting the thermal response of the graphene to the laser-heating effect. Thermal expansion only happens around the small laser-heating area.

graphene is higher, say 2000 W m^{-1} K^{-1}, the interfacial thermal resistance would be as high as $1.05^{+0.21}_{-0.21} \times 10^{-4}$ Km^2 W^{-1}. In the case of the above in-plane thermal resistance analysis for the graphene–SiC system the interfacial thermal resistance obtained by the Joule-heating experiment is used. If the thermal resistance value from the laser-heating experiment is used, the calculation iterations need to use updated results from the laser-heating experiment by assuming that interfacial thermal resistance is the same across the whole sample, regardless of whether the region is laser heated or not. Using the iteration, for an assumed graphene thermal conductivity of 1000 W m^{-1} K^{-1}, the graphene–SiC thermal resistance was determined to be $1.01^{+1.23}_{-0.59} \times 10^{-4}$ Km^2 W^{-1}. In this interfacial thermal resistance analysis the laser-heating spot is rectangular, while an effective circular heating area is assumed in order to simply the evaluation. This could introduce uncertainty in the values reported in the above discussion. Nonetheless, the high interfacial thermal resistance obtained by the pure laser-heating characterization qualitatively agrees with that of the Joule-heating measurement. The difference between them could be induced by the larger temperature rise in the laser-heating experiment. The higher temperature of graphene and the larger temperature difference between graphene and SiC will give rise to more interfacial thermal expansion and mismatch, making the interfacial thermal resistance larger. Recent work by Mak et al. shows that the absorption of laser light in a graphene layer is affected by many body effects, the result of which is a laser absorption ratio that is a function of wavelength.[35] In their results, the absorption at our wavelength is higher than 2.3%. If a higher value is used for our wavelength, the measured thermal resistance should be lower than the value reported above.

Figure 7b shows a schematic that depicts the thermal response of the graphene to the laser-heating experiment. Unlike with Joule heating, the thermal-expansion effect happens mainly in the small laser-heated area, resulting in huge mismatch effect and a high thermal resistance. Other unheated regions where there is less or no mismatch effect would have higher interfacial thermal conductance. The majority of the absorbed laser energy dissipates in the in-plane direction, then down to the substrate in other unheated regions. The temperature rise of the laser-heated region is higher than that in the Joule-heating experiment. Therefore, the resulting thermal-expansion effect would be stronger, explaining why the measured thermal resistance is larger.

Notably, there is potential concern about unexpected heating from the laser, which might affect the accuracy with which the heating density is computed. To reduce this effect, only 10 percent of the laser energy was used, which ensures a light intensity good enough to stimulate a Raman signal while avoiding unwanted heating effects. In addition, as observed in the laser-heating experiment, the sound Raman spectra emerge only at low focal levels when laser heating is not significant. The Raman intensity decreases as the focal level becomes higher, which means that a stronger heating effect happens. In our experiment, to determine the Raman peak positions with a high degree of accuracy, the Raman signal is always carefully adjusted to be the strongest for each acquisition. In this case, the heating effect from the laser should be minimized. Even if there is little photon heating in the sample, this effect could be cancelled out as the same heating exists in both the calibration and measurement experiments. Therefore, we submit that there is negligible uncertainty induced by the laser-heating effect in the Joule-heating measurement.

In addition, the thermal stress in the sample during the heating process could affect the results, since not only temperature, but also stress, is a factor leading to the peak shift. To evaluate the result obtained by using the frequency method, the width method, which measures the full width at half maximum

© 2011 Wiley-VCH Verlag GmbH & Co. KGaA, Weinheim

small NANO MICRO

(FWHM) of the peak, is employed to study the interfacial thermal resistance. Since peak width is closely related to the phonon lifetime, which in turn is only influenced by temperature,[36] this method can be effectively used to determine the temperature and then to evaluate the thermal resistance. However, as mentioned in the introduction section, the sensitivity of this method is low compared to the frequency method. To overcome this challenge, more experimental data was collected in order to reduce the error. The Lorentz function is used to fit Raman peaks (G-band of graphene and E_2 peak of SiC) in order to determine the peak width. The processed data using this method is shown in **Figure 8**, including the temperature calibration of peak width and the measurement result for the change of width with heating power. For calibration, temperature coefficients of graphene and SiC are determined as 0.0127 and 0.0087 cm^{-1} °C^{-1}. In the interfacial thermal resistance measurement, the slopes for graphene and SiC are obtained as 0.1614 and 0.0885 cm^{-1} W^{-1}, respectively. Thereby, the thermal resistance is determined as 3.52×10^{-5} K m^2 W^{-1}, which is slightly smaller than the value measured using the frequency method. In the laser-heating experiment, temperatures of graphene and SiC are determined to be 390 and 204 °C, respectively. Correspondingly, the thermal resistance was evaluated as 8.57×10^{-5} K m^2 W^{-1}, which agrees well with the results from the Joule-heating experiment. The results show that the thermal-stress effect can contribute to Raman peak shifts, and impart a small error in the determination of the temperatures using the frequency method. Nevertheless, the similar results obtained by these two methods confirm the large thermal resistance between graphene and SiC. In addition, the fact that larger values always appear in laser-heating experiment, confirms that high temperatures during the measurement (which leads to elevated thermal expansion effect) are an important factor, which results in the anomalous thermal resistance at the interface.

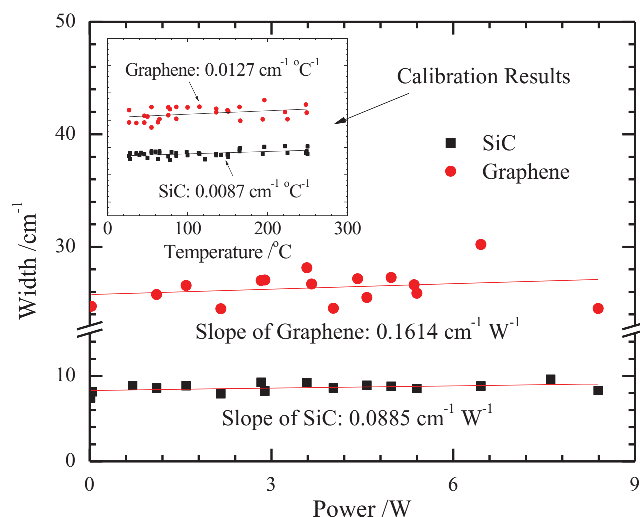

Figure 8. Interfacial thermal resistance characterization based on the peak-width method of Raman thermometry. In calibration, the temperature coefficients of graphene and SiC are determined as 0.0127 and 0.0087 cm^{-1}°C^{-1}, and the slopes for graphene and SiC in the measurement experiment are obtained as 0.1614 and 0.0885 cm^{-1} W^{-1}, respectively.

Other uncertainties of the Joule-heating measurement come from radiative heat and convective losses from the graphene surface, which should be included as the sample is exposed to air. For the radiation effect, the total radiation thermal resistance between the graphene sheet and the surroundings can be expressed as $R_r \approx 1/\left[A\varepsilon 0(T+T_s)(T^2+T_s^2)\right]$, where T is the graphene temperature and T_s (≈300 K) is the surrounding temperature, ε is the graphene surface emissivity, and σ is the Stefan–Boltzmann constant. Considering the extreme situation for $\varepsilon \approx 1$, the highest heat radiation loss is only 1.2% of the total heating power. The radiation thermal resistance is calculated as 4.56×10^{-2} K m^2 W^{-1}, which is 860 times higher than the graphene–SiC contact resistance. The convection heat-transfer thermal resistance is deduced as $1/h$, where h is the convection coefficient. The situation in our experiment is regarded as natural convection and the h value changes with temperature due to the buoyancy force of air.[33] The value of h is derived as $k \cdot Nu/L$, where k is the thermal conductivity of air; L the effective length of the surface, and the Nusselt number (Nu) is determined by the expression ($0.54 Ra_L^{1/4}$), where the Rayleigh number (Ra_L) depends on the temperature. The highest value of h, which occurs at the highest temperature, is calculated to be 5.28 W K^{-1} m^{-2}. The corresponding thermal resistance for heat convection is 1.89×10^{-1} K m^2 W^{-1}. The combined thermal resistance of convection and radiation is still 694 times the graphene–SiC contact resistance, indicating that there is very little heat loss through these two effects and that the uncertainties induced by them may be considered negligible.

In this work, the spatial resolution of the thermal probe concept is limited by the material structure not the laser focusing, since Raman peaks (structure-dependence) are used for thermal sensing. Therefore, if different materials are patterned in space with nanometer resolution, since each material will have a different Raman peak for its atomic structure, Raman spectroscopy can be used simultaneously to distinguish and measure their temperatures. This provides unprecedented resolution and capacity to probe the temperature on both sides of materials interface, and characterize the interfacial thermal resistance. In this work, the temperature measurement in SiC has about a 12 μm resolution, which is determined by the focusing depth of the excitation laser in the Raman spectrometer. If a thinner SiC film is patterned on a different substrate (e.g., Si), and graphene is grown/patterned on SiC, then the temperature measurement could achieve high resolution on both sides of the graphene–SiC interface.

4. Conclusion

In this work, the thermal contact resistance between epitaxial graphene and 4H-SiC was explored using Raman thermometry combined with Joule heating. Through simultaneous analysis of the Raman peaks of graphene and SiC we were able to distinguish and measure their temperatures at the same time. This unique method of probing the temperature can achieve nanoscale resolution in terms of separating the graphene temperature from that of its

 © 2011 Wiley-VCH Verlag GmbH & Co. KGaA, Weinheim

immediate adjacent substrate. The result showed that the thermal contact resistance between tri-layer graphene and 4H-SiC was as high as $5.30^{+0.46}_{-0.46} \times 10^{-5}$ Km^2 W^{-1}. An independent laser-heating experiment was also conducted to characterize the graphene–SiC interfacial thermal resistance, and a value of $1.01^{+1.23}_{-0.59} \times 10^{-4}$ Km^2 W^{-1} was obtained, qualitatively agreeing with the Joule heating result. The larger temperature difference between graphene and SiC in the laser-heating experiment led to larger interfacial thermal expansion mismatch, thereby giving rise to more interface separation/delamination and a higher thermal resistance. To address the stress effect during the heating experiment, the parallel peak width method was employed to study the interfacial thermal resistance, which yielded 3.52×10^{-5} and 8.57×10^{-5} K m^2 W^{-1} for Joule-heating and laser-heating experiments, respectively. Our MD simulation of a single-layer graphene on SiC gave interfacial thermal contact resistances of $7.01^{+1.05}_{-1.05} \times 10^{-10}$ and $8.47^{+0.75}_{-0.75} \times 10^{-10}$ Km^2 W^{-1} for surface heat fluxes of 3×10^9 and 1×10^{10} W m^{-2}, respectively. The measured anomalous thermal contact resistance was mainly attributed to the significantly enhanced phonon scattering effect from the structural change at the interface induced by the local thermal expansion mismatch. The thermal probing technique reported in this work provides a promising way to realize nanometer or subnanometer resolution temperature measurements in space.

5. Experimental Section

The semi-insulating 4H-SiC substrate was obtained from Cree, USA with dimensions 3.5 mm × 4.5 mm × 0.5 mm. Epitaxial graphene is grown uniformly on the C-face of the SiC by heating the sample to above 1300°C under ultra-high vacuum. The fabrication is conducted at Graphene Works, with the sample image shown in Figure 3. The Raman spectrometer employed in this work was installed with 532 nm excitation laser and a spectrometer with a 1.75 cm^{-1} pixel resolution. In the experiment, a 50× long working distance lens with high-level correction for chromatic aberration is used. The focal plane of the laser beam through this lens is 2 μm × 4 μm, as shown in Figure 1. To get sound Raman signal, a 40 s integration time is used throughout the whole experiment. In the calibration, the sample temperature is measured by using a T-type thermocouple, which is placed very close to the sample to ensure accuracy. The calibration measurement was conducted from room temperature to 250 °C with an excitation laser irradiated on the center of the sample to eliminate the effect of heat loss at the edges. Corresponding Raman spectra are saved spontaneously to establish the relationship between the temperature and the Raman peaks.

In the Joule-heating experiment, two electrode probes are used to connect the ends of the graphene layer. Very little silver paste is adhered at the contact points to reduce the contact resistance. A bulk silicon piece acting as a heat sink is placed under the sample to ensure sound heat conduction from the SiC substrate. The same point measured in the calibration is used in the thermal contact-resistance experiment, which is marked in Figure 3. The resistance of the sample was 442 Ω and different heating powers up to 8 W were applied.

Acknowledgements

Support of this work managed by Dr. Pani (Chakrapani) Varanasi from the Army Research Office is gratefully acknowledged. Also X.W. very much appreciates the helpful discussion with Dr. Varanasi and his inspiring comments on the experiment.

[1] a) K. S. Novoselov, A. K. Geim, S. V. Morozov, D. Jiang, Y. Zhang, S. V. Dubonos, I. V. Grigorieva, A. A. Firsov, *Science* **2004**, *306*, 666; b) K. S. Novoselov, A. K. Geim, S. V. Morozov, D. Jiang, M. I. Katsnelson, I. V. Grigorieva, S. V. Dubonos, A. A. Firsov, *Nature* **2005**, *438*, 197; c) A. K. Geim, K. S. Novoselov, *Nat. Mater.* **2007**, *6*, 183; d) Y. Zhang, Y.-W. Tan, H. L. Stormer, P. Kim, *Nature* **2005**, *438*, 201.

[2] a) K. I. Bolotin, K. J. Sikes, J. Hone, H. L. Stormer, P. Kim, *Phys. Rev. Lett.* **2008**, *101*, 096802; b) X. Du, I. Skachko, A. Barker, E. Y. Andrei, *Nat. Nanotechnol.* **2008**, *3*, 491; c) Y. Q. Wu, P. D. Ye, M. A. Capano, Y. Xuan, Y. Sui, M. Qi, J. A. Cooper, T. Shen, D. Pandey, G. Prakash, R. Reifenberger, *Appl. Phys. Lett.* **2008**, *92*, 092102; d) A. A. Balandin, S. Ghosh, W. Bao, I. Calizo, D. Teweldebrhan, F. Miao, C. N. Lau, *Nano Lett.* **2008**, *8*, 902.

[3] a) S. Ghosh, I. Calizo, D. Teweldebrhan, E. P. Pokatilov, D. L. Nika, A. A. Balandin, W. Bao, F. Miao, C. N. Lau, *Appl. Phys. Lett.* **2008**, *92*, 151911; b) J.-U. Lee, D. Yoon, H. Kim, S. W. Lee, H. Cheong, *Phys. Rev. B* **2011**, *83*, 081419; c) S. Ghosh, W. Bao, D. L. Nika, S. Subrina, E. P. Pokatilov, C. N. Lau, A. A. Balandin, *Nat. Mater.* **2010**, *9*, 555.

[4] a) D. L. Nika, E. P. Pokatilov, A. S. Askerov, A. A. Balandin, *Phys. Rev. B* **2009**, *79*, 155413; b) J. Hu, X. Ruan, Y. P. Chen, *Nano Lett.* **2009**, *9*, 2730; c) D. L. Nika, S. Ghosh, E. P. Pokatilov, A. A. Balandin, *Appl. Phys. Lett.* **2009**, *94*, 203103.

[5] a) Z. H. Ni, W. Chen, X. F. Fan, J. L. Kuo, T. Yu, A. T. S. Wee, Z. X. Shen, *Phys. Rev. B* **2008**, *77*, 115416; b) C. Berger, Z. Song, X. Li, X. Wu, N. Brown, C. Naud, D. Mayou, T. Li, J. Hass, A. N. Marchenkov, E. H. Conrad, P. N. First, W. A. de Heer, *Science* **2006**, *312*, 1191.

[6] a) K. V. Emtsev, F. Speck, T. Seyller, L. Ley, J. D. Riley, *Phys. Rev. B* **2008**, *77*, 155303; b) A. Mattausch, O. Pankratov, *Phys. Rev. Lett.* **2007**, *99*, 076802; c) U. Starke, C. Riedl, *J. Phys.: Condens. Matter* **2009**, *21*, 134016.

[7] M. Freitag, M. Steiner, Y. Martin, V. Perebeinos, Z. Chen, J. C. Tsang, P. Avouris, *Nano Lett.* **2009**, *9*, 1883.

[8] M. A. Panzer, K. E. Goodson, *J. Appl. Phys.* **2008**, *103*, 094301.

[9] Z. Chen, W. Jang, W. Bao, C. N. Lau, C. Dames, *Appl. Phys. Lett.* **2009**, *95*, 161910.

[10] A. J. Schmidt, K. C. Collins, A. J. Minnich, G. Chen, *J. Appl. Phys.* **2010**, *107*, 104907.

[11] Y. Yue, G. Eres, X. Wang, L. Guo, *Appl. Phys. A* **2009**, *97*, 19.

[12] a) R. F. Wallis, M. Balkanski, *Many-Body Aspects of Solid State Spectroscopy*, North-Holland Physics, Amsterdam **1986**; b) W. H. Weber, *Raman Scattering in Materials Science*, Springer, New York **2000**.

[13] a) A. C. Ferrari, J. C. Meyer, V. Scardaci, C. Casiraghi, M. Lazzeri, F. Mauri, S. Piscanec, D. Jiang, K. S. Novoselov, S. Roth, A. K. Geim, *Phys. Rev. Lett.* **2006**, *97*, 187401; b) J. C. Burton, L. Sun, M. Pophristic, S. J. Lukacs, F. H. Long, Z. C. Feng, I. T. Ferguson, *J. Appl. Phys.* **1998**, *84*, 6268.

[14] D. Graf, F. Molitor, K. Ensslin, C. Stampfer, A. Jungen, C. Hierold, L. Wirtz, *Nano Lett.* **2007**, *7*, 238.

[15] I. Calizo, A. A. Balandin, W. Bao, F. Miao, C. N. Lau, *Nano Lett.* **2007**, *7*, 2645.

[16] Z. H. Ni, H. M. Wang, J. Kasim, H. M. Fan, T. Yu, Y. H. Wu, Y. P. Feng, Z. X. Shen, *Nano Lett.* **2007**, *7*, 2758.

© 2011 Wiley-VCH Verlag GmbH & Co. KGaA, Weinheim

small NANO MICRO

[17] C. Thomsen, S. Reich, *Phys. Rev. Lett.* **2000**, *85*, 5214.
[18] H. Harima, T. Hosoda, S. Nakashima, *J. Electro. Mater.* **1999**, *28*, 141.
[19] a) L. Zhang, Z. Jia, L. Huang, S. O'Brien, Z. Yu, *J. Phys. Chem. C* **2008**, *112*, 13893; b) M. J. Allen, J. D. Fowler, V. C. Tung, Y. Yang, B. H. Weiller, R. B. Kaner, *Appl. Phys. Lett.* **2008**, *93*, 193119.
[20] N. Bonini, R. Rao, A. M. Rao, N. Marzari, J. Menéndez, *Phys. Status Solidi B* **2008**, *245*, 2149.
[21] M. Balkanski, R. F. Wallis, E. Haro, *Phys. Rev. B* **1983**, *28*, 1928.
[22] H.-K. Lyeo, D. G. Cahill, *Phys. Rev. B* **2006**, *73*, 144301.
[23] J.-W. Jiang, J.-S. Wang, B. Li, *Phys. Rev. B* **2009**, *80*, 205429.
[24] J. Rohrl, M. Hundhausen, K. V. Emtsev, T. Seyller, R. Graupner, L. Ley, *Appl. Phys. Lett.* **2008**, *92*, 201918.
[25] Z. Li, R. C. Bradt, *J. Appl. Phys.* **1986**, *60*, 612.
[26] N. Ferralis, R. Maboudian, C. Carraro, *Phys. Rev. Lett.* **2008**, *101*, 156801.
[27] G. Chen, *Int. J. Therm. Sci.* **2000**, *39*, 471.
[28] A. J. Schmidt, X. Chen, G. Chen, *Rev. Sci. Instrum.* **2008**, *79*, 114902.
[29] R. R. Nair, P. Blake, A. N. Grigorenko, K. S. Novoselov, T. J. Booth, T. Stauber, N. M. R. Peres, A. K. Geim, *Science* **2008**, *320*, 1308.
[30] C. Faugeras, B. Faugeras, M. Orlita, M. Potemski, R. R. Nair, A. K. Geim, *ACS Nano* **2010**, *4*, 1889.
[31] W. Cai, A. L. Moore, Y. Zhu, X. Li, S. Chen, L. Shi, R. S. Ruoff, *Nano Lett.* **2010**, *10*, 1645.
[32] G. L. Harris, *Properties of Silicon Carbide*, The Institution of Electrical Engineers, London **1995**.
[33] F. P. Incropera, D. P. Dewitt, T. L. Bergman, A. S. Lavine, *Fundamentals of Heat and Mass Transfer*, John Wiley & Sons, Inc., New York **2007**.
[34] P. Nemes-Incze, Z. Osváth, K. Kamarás, L. P. Biró, *Carbon* **2008**, *46*, 1435.
[35] K. F. Mak, J. Shan, T. F. Heinz, *Phys. Rev. Lett.* **2011**, *106*, 046401.
[36] T. Beechem, S. Graham, S. P. Kearney, L. M. Phinney, J. R. Serrano, *Rev. Sci. Instrum.* **2007**, *78*, 061301.

Received: August 7, 2011
Published online: October 13, 2011

 © 2011 Wiley-VCH Verlag GmbH & Co. KGaA, Weinheim